JOURNAL OF SPACECRAFT AND ROCKETS
Vol. 34, No. 4, July–August 1997

Fluid Dynamics of Hypersonic Forward-Facing Cavity Flow

W. A. Engblom* and D. B. Goldstein†
University of Texas at Austin, Austin, Texas 78712
and
D. Ladoon‡ and S. P. Schneider§
Purdue University, West Lafayette, Indiana 47907-1282

Hypersonic flow over the nose of a blunt body with a forward-facing cylindrical cavity is studied. Extensive numerical results involving a wide range of cavity depths are verified by experimental runs including a new set of runs performed in a quiet flow supersonic tunnel at Mach 4. It is shown that freestream noise is the mechanism that drives resonant pressure oscillations within relatively shallow cavities. Numerical results and conventional tunnel experiments show that deeper cavities oscillate strongly without freestream noise. For shallow cavities the sensitivity of cavity amplification, i.e., the relative strength of resonant pressure oscillations, to the characteristics of freestream noise (frequency, amplitude, perturbation variable), cavity geometry (depth, geometric scale, lip radius), Mach number, viscous effects, and thermal wall boundary condition is studied. There is a strong dependence of oscillation strength on freestream noise frequency. Oscillation strength increases nearly proportionally to input noise amplitude, increases rapidly with cavity depth, and increases with Mach number but levels off at high Mach numbers. The pressure oscillations exhibit behavior analogous to that of a damped harmonic oscillator.

Nomenclature

a, C_o	= speed of sound, m/s
D	= cavity diameter, cm
f	= input frequency, Hz
f_{opt}	= frequency at optimum pressure amplification, Hz
f_1	= primary mode frequency, Hz
G	= pressure amplification at cavity base
L	= cavity length or depth, cm
L^*	= characteristic length, cm
M_∞	= freestream Mach number
P_{base}	= cavity base pressure, Pa
$P_{\text{base,rms}}$	= cavity base pressure rms
P_{mean}	= mean cavity base pressure, Pa
P_{t_2}	= stagnation pressure behind normal shock, Pa
P_∞	= freestream static pressure, Pa
$P_{\infty,\text{rms}}$	= freestream static pressure rms
T_0	= steady-flow stagnation temperature, K
ρ_∞	= freestream density, kg/m^3

Introduction

THERE is recent evidence that introducing an axial cavity in the nose region of a hypersonic vehicle (Fig. 1) could result in a local reduction in peak heating.[1] Strong longitudinal pressure oscillations are generated within the cavity to induce bow-shock oscillations, which provide the cooling mechanism. Consequently, there is a need to understand the fluid dynamics of hypersonic forward-facing cavity flow.

Early experimental studies in conventional wind tunnels involving supersonic and hypersonic flows over concave nose configurations indicated that the resulting flow can be steady or unsteady depending on the Mach number and angle of attack.[2,3] The unsteady flows, characterized by nonaxisymmetric and sporadic bow-shock behavior, generally occurred at higher Mach numbers and lower angles of attack.

Marquart et al.[4] focused on the dynamics of the detached bow shock and on acoustic resonance for models with conical nose cavities and bulbous lips at $M_\infty = 10$. They found that the rms levels of the fluctuating pressure along the cavity wall increased toward the cavity base. Huebner and Utreja[5] presented a detailed description of the bow-shock behavior associated with a similar body at $M_\infty = 10$. Although they observed a violent bow-shock instability for one set of conditions during the test, the primary behavior was a stable, periodically oscillating bow shock.

Numerical studies involving similar flow geometries agree that the unsteady nature depends on particular conditions.[6,7] Bastianon[7] simulated viscous Mach 3 flow over concave configurations with various depths and found that for depths greater than 40% of the cylindrical body radius the flow oscillates in a repeatable manner, but for shallow cavities the flow becomes steady. He found that the oscillation wavelength corresponds to four times the distance from the cavity base to the mean bow-shock position. Yang and Antonison[8] performed a numerical investigation using the Euler equations of bow-shock behavior for conical nose cavities with different fields of view (FOV) at $M_\infty = 6.6$. They found that the strength of oscillatory bow-shock motion decreases as cavity FOV increases (or cavity depth decreases). For a large FOV of 60 deg, the transients quickly dampened out to a steady-state flow.

A joint numerical and experimental effort[9] at $M_\infty = 5$ showed that pressure oscillations at the cavity base are typically planar. In the experiments, oscillation strength was found to increase with cavity depth for shallow cavities and deep cavities but consistently exhibited wild behavior for medium-depth cavities with a cavity length-to-diameter (L/D) ratio of 0.4–0.7. Yuceil and Dolling[10] found that the bow shock typically oscillates axisymmetrically, except for the medium-depth cases.

The objective of the present study is to examine the fluid dynamics of hypersonic flow about a forward-facing cavity, expand the range of parameters studied, and provide cleaner numerical and wind-tunnel experiments. All previous experimental tests were conducted in conventional facilities, which produce a significant amount of freestream noise due to acoustic radiation from the turbulent boundary layers normally present on the tunnel walls.

Methodology

This paper presents results from a study of the fluid mechanics of axial cavity flows. Experimental results obtained from recent work

Received Oct. 2, 1996; revision received March 16, 1997; accepted for publication March 17, 1997.

*Graduate Research Assistant, Center for Aeromechanics Research, Department of Aerospace Engineering and Engineering Mechanics. Member AIAA.

†Assistant Professor, Center for Aeromechanics Research, Department of Aerospace Engineering and Engineering Mechanics. Member AIAA.

‡Graduate Research Assistant, School of Aeronautics and Astronautics. Student Member AIAA.

§Associate Professor, School of Aeronautics and Astronautics. Senior Member AIAA.

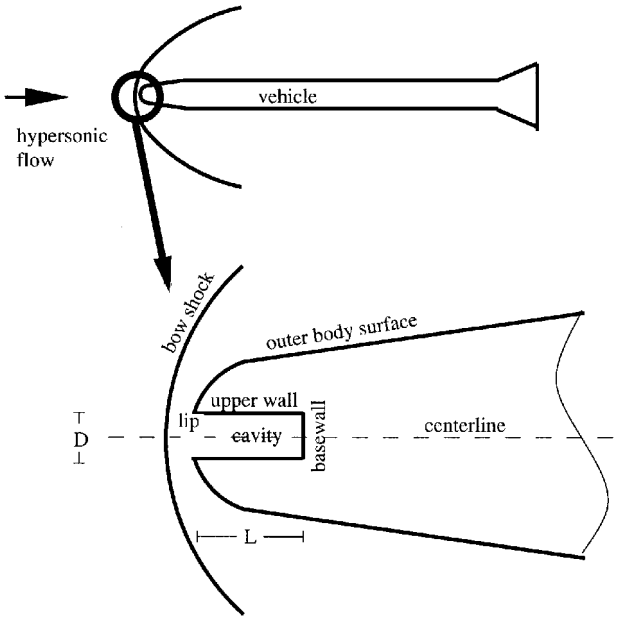

Fig. 1 Schematic of axial cavity in the nose region of a hypersonic vehicle.

conducted in the Purdue Quiet Flow Ludwieg Tube (PQFLT) are described. Similar body geometry and freestream conditions are used in both numerical simulations and the experiments.

Computer Code

The commercial code INCA[11] (licensed from Amtec Engineering) was used for this study. INCA is a finite volume code that utilizes flux splitting with upwinding to capture strong shocks. Fluxes are computed with the flux splitting of Steger and Warming.[12] INCA offers a variation of the lower–upper successive Gauss–Seidel (LU-SGS) implicit solver to calculate unsteady flows. This algorithm permits much larger time steps than a simple Euler step method by performing a sufficient number of subiterations at each time step. It is also second-order accurate in time and space. Only structured grids are employed, in view of the simple geometries involved.

Numerical Assumptions

The numerical model is a hemispherically blunted cylinder containing a cylindrical cavity to model the PQFLT experiments. The numerical body diameter is 2.54 cm, and the cavity diameter D is 1.27 cm. The cavity L/D is varied between 0 and 2.0. The experimental cavity lip is quite sharp ($\sim$0.1-mm lip radius), and it is numerically modeled as infinitely sharp. The Mach number is 4, and the rms freestream noise is approximately 0.048% (see "Experimental Setup").

For all other numerical parameter studies presented herein, the body geometry and freestream conditions are consistent with those of recent experiments[9] conducted in the University of Texas at Austin (UT) Mach 5 blowdown facility at Pickle Research Center (PRC). In these cases, the body diameter is 5.08 cm and the cavity diameter (D) is 2.54 cm. The cavity L/D ratio is again varied between 0 and 2.0. The cavity lip is sharp ($\sim$0.1-mm radius) and is numerically modeled as either 0.1-mm radius or infinitely sharp. The Mach number is 5, and the rms freestream noise variation is approximately 1.15%.

Several simplifying assumptions are made in the simulations. The flow is assumed axisymmetric.[5,9,10] Because of the small scale of the flowfield (nose region), laminar flow is assumed. The freestream Reynolds number is approximately 5.0×10^5/cm at Mach 5 and an order of magnitude lower at Mach 4. The actual Reynolds number (per centimeter) is much smaller along the body surface inside the cavity and outside the cavity near the lip because of the low-speed flow. Because the characteristic flow lengths are less than 1 cm and a favorable pressure gradient is present along the cavity wall, transition is not expected to occur within regions of interest unless the oscillations within the cavity cause the flow to trip. (There is no experimental evidence to date that the flow within the cavity is either laminar, transitional, or turbulent.) The wall temperature is assumed isothermal ($T_{\text{wall}} = 300$ K) unless otherwise specified. The minimum and maximum flow temperatures in the Mach 4 and 5 simulations presented here always remain between 64 and 530 K. Because the specific heats of air change less than 5% over this temperature range, the flow is assumed to be calorically perfect.

Numerical Procedure

The unsteady pressure field solution can be obtained with a relatively coarse grid near the body surface (10^{-2}-mm surface cell thickness—this is too coarse to determine heat transfer rates accurately). Finer resolution of the boundary layer has a negligible effect on the strength of pressure oscillations within the cavity. A moderately fine grid, however, is needed to resolve the bow-shock position, i.e., 80×80 cells. These grid parameters were determined from a grid refinement study. The resolution of acoustic waves must also be considered. An aeroacoustics guideline is that six to eight cells per wavelength is required to resolve linear acoustic waves (to minimize dispersion and dissipation).[13] Because INCA is not optimized for aeroacoustics purposes, and the waves are nonlinear, this requirement may be several times higher (perhaps 40 cells per wavelength). Each grid easily meets the latter requirement (by a factor of 10 or more) for proper resolution of the resonant frequencies of interest. Nevertheless, grid resolution checks were performed.

Generally a two-zone grid with an infinitely sharp lip is implemented (one zone contains only the cavity region). Sometimes, however, a single-zone grid with a 0.1-mm lip radius lip is used to examine surface heat transfer effects.[1] Simulations for a representative case ($L/D = 0.75$, Mach 5) with both types of grids indicate that oscillation strength is virtually unaffected by the grid type and whether the lip radius is 0 or 0.1 mm. The single-zone grids typically produce more high-frequency numerical noise than the two-zone grids. However, this numerical noise is of very low energy and exists at much higher frequencies (>100 kHz) than the resonant frequencies (between 1 and 10 kHz).

Experimental Setup

The PQFLT is a Mach 4 impulse wind tunnel.[14] A Ludwieg tube is a long pipe with a converging–diverging nozzle on one end through which flow exits into the test section and diffuser. The Purdue driver is 20.7 m long and 30 cm in diameter. A smooth contraction tapers from the driver tube to the throat, which is in turn followed by a Mach 4 rectangular nozzle. The nozzle is polished to a smooth surface finish throughout. Within the inviscid core flow of the nozzle is a test rhombus of uniform quiet flow. A practical criterion for quiet flow is that the rms of the pitot-pressure fluctuations must be less than 0.05% of the mean pitot pressure.[15] The forward part of the test rhombus corresponds to the start of uniform supersonic flow. The end of the test rhombus is defined by the region affected by the turbulent spots that develop on the tunnel walls. At modest driver pressures (less than one atmosphere), the flow in the nozzle is laminar and rms total pressure fluctuations are about 0.05%. This corresponds to noise levels that are typically an order of magnitude less than those of conventional facilities.

The Reynolds number in the test section is determined by the stagnation, or driver tube, pressure. The run time is about 3.5 s. The stagnation pressure drops by approximately 35%, or 1% per 100 ms, during this 3.5-s period.[16] For the PQFLT data reported here, the tunnel driver pressure and stagnation temperature were 1 atm and 293 K.

Test Model and Equipment

The nose-cone model used in the PQFLT experiments, shown in Fig. 2, consists of a 1.905-cm-diam cylinder with a hemispherical tip. A 0.953-cm-diam hole along the axis of the nose cone served as a forward-facing cavity. The cavity length L was varied by changing the axial position of the steel insert. The cavity L/D ratios used ranged from 0.0 to 1.848. A Kulite® model XCQ-062-25A pressure transducer was mounted on the centerline of the cavity base via a 10–32 brass screw.

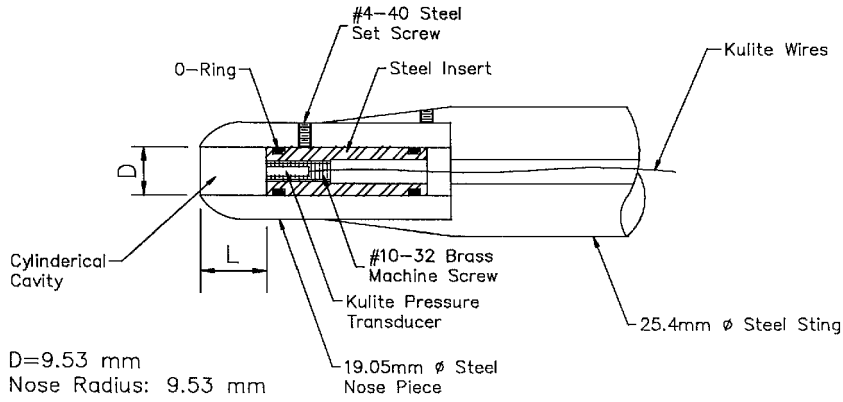

Fig. 2 Sectional view of cavity model used in Mach 4 PQFLT runs.

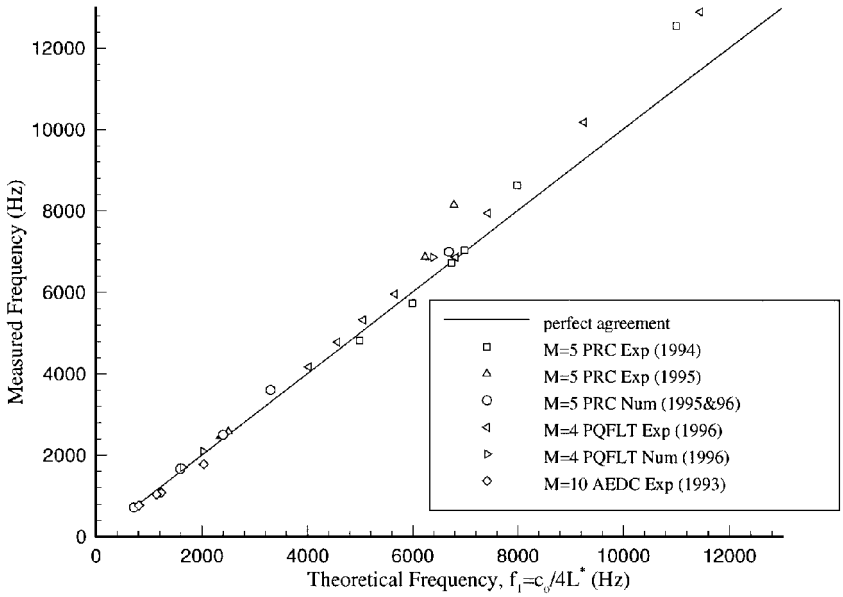

Fig. 3 Cavity frequency response.

Results

Primary Organ-Pipe Frequency

Oscillating pressure levels within a cavity are a dominant experimental flow feature in forward-facing cavity configurations. Resonant frequencies are obtained by spectral analysis of the fluctuating pressure measurements made in the cavity. Most of the energy of the oscillations is contained in the primary mode frequency.[4,9] Primary frequencies (f_1) can be estimated a priori from a simple linear relation derived from the one-dimensional wave equation in classic organ-pipe theory by considering only the characteristic wavelength λ and the speed of sound a inside the cavity:

$$f_1 = a/\lambda \tag{1}$$

Time-accurate flow animations for cavities of modestly large diameter (described later) indicate that pressure waves travel between the bow shock and the base of the cavity. These pressure waves are reflected off the base wall and inverted off the bow shock. Consequently, an appropriate λ is four times the distance between the mean bow shock location and the cavity base along the centerline (L^*). Numerical steady flowfield solutions indicate that the flow is virtually stagnant inside the cavity. Hence, the speed of sound can be estimated assuming the gas temperature inside the cavity is approximately the stagnation temperature T_0 of the flow. Thus,

$$f_1 = \frac{\sqrt{\gamma R T_0}}{4L^*} \tag{2}$$

As seen in Fig. 3, this equation clearly provides good agreement with primary frequencies derived from various experimental runs and time-accurate numerical simulations. The shock standoff distances used in Eq. (2) are obtained from either schlieren photographs or steady-flow computational fluid dynamics solutions. Note that the straight line with slope of 1 represents perfect agreement between the theoretical [Eq. (2)] and measured frequencies. The agreement is generally best for the deepest cavities. (L^* is less ambiguous when the cavity depth is much greater than the cavity radius.)

Mechanisms of Resonance

To study the mechanisms of resonance, we first compare numerical simulation results to experimental results for the same body configuration and freestream conditions at Mach 5. The numerical input noise is adapted from broad-spectrum white-noise data obtained from pitot stagnation pressure P_{t2} measurements on a blunt body in the UT Mach 5 blowdown facility. This data set is rescaled to provide a numerical inflow noise history and retain the same rms variation of approximately $\pm 1.15\%$. The numerical noise consists of in-phase variations of static pressure and density (temperature is held constant) and is effectively represented as one-dimensional plane waves having negligible radial variations. Numerical simulations involve more than 50 oscillations at the primary frequency. The rms of base pressure fluctuations is estimated from the base pressure history after the oscillations are stable, i.e., after the initial 3–10 cycles in most cases. Another set of numerical simulations without inflow noise (steady inflow conditions) is also computed.

Input waves typically result in large stagnation pressure oscillations at the base of the cavity. The amplification G is defined as the ratio of the output (centerline base pressure) rms amplitude to the input (freestream) rms amplitude:

$$G = \frac{P_{\text{base,rms}}}{P_{\infty,\text{rms}}} \tag{3}$$

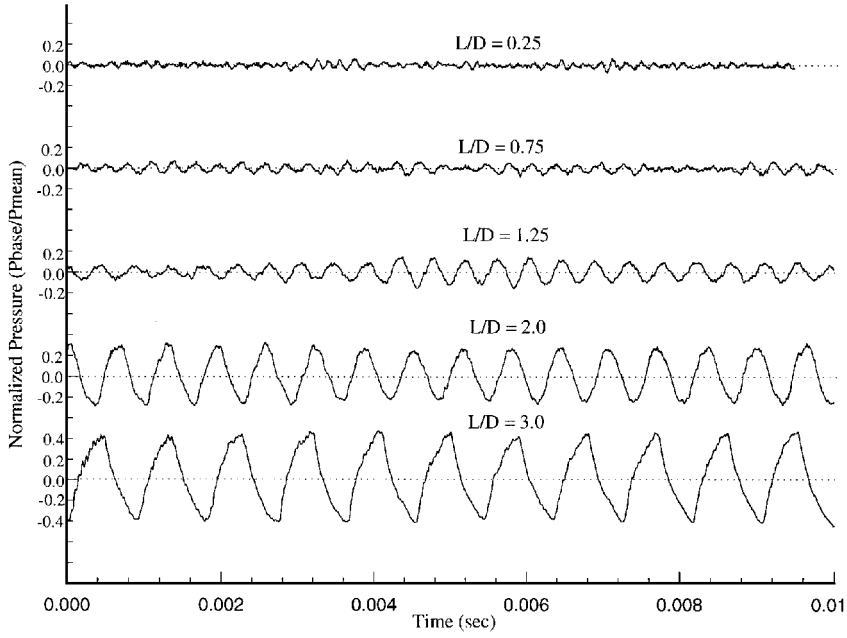

Fig. 4 Numerical base pressure signals (Mach 5 tunnel conditions).

For example, if a cavity driven with a perturbation input rms of $\pm 1.15\% P_\infty$ and $\pm 1.15\% \rho_\infty$ produces an output rms of $\pm 23.0\% P_{t_2}$ at the cavity base; this results in an amplification of 20.

The numerical results, i.e., portions of the base pressure histories, for various cavity depths at Mach 5 are shown in Fig. 4. Based on power spectrum analysis, most of the oscillation energy is contained within a small band near f_1. Note that the oscillations become cleaner, i.e., more sinusoidal, and stronger with increasing cavity depth. The $L/D = 3.0$ case exhibits quasistatic bow-shock motion in which the bow shock remains fixed at the mouth of the cavity during inflow and at an upstream position during outflow and moves abruptly between these two positions. This motion is reflected in the shark-tooth shape of the base pressure trace.

Figure 5a illustrates how amplification grows with cavity depth in numerical simulations and experiments at Mach 5 (Ref. 17). When freestream noise is present, both the numerics and the experiments show a gradual increase of oscillation strength with cavity depth for shallow cavities ($L/D \leq 1.0$). The numerical estimates for shallow cavities involve some statistical uncertainty due to the limited duration of the simulation. Because the experiments involving medium-depth cavities ($0.4 \leq L/D \leq 0.7$) exhibit two modes of resonance,[9] the rms estimate is somewhat ambiguous and is not included (dotted line). This behavior is strongly asymmetric and cannot be directly compared with axisymmetric numerical results.

A qualitative change in the curve occurs near $L/D = 1.0$. Figure 5a shows that the slope of the amplification curve increases dramatically ($L/D > 1.0$) in both the experiments and numerical simulations. However, the numerical model produces a smaller estimate of the oscillations that occur in the experiments. Some of the difference may be due to numerical dissipation of the fast-moving bow shock and strong waves within the cavity; however, a rigorous spatial and temporal sensitivity study of the $L/D = 2.0$ case indicates the numerical solution is converged. The numerical and experimental results are quite sensitive to cavity depth near $L/D = 1$, and it is reasonable to expect that these results are very sensitive to many other parameters.

Figure 5b illustrates how amplification grows with cavity depth in numerical simulations at Mach 5 with and without freestream noise. Numerical oscillations are only obtained for relatively shallow cavities ($L/D < 1.25$) by introducing freestream noise. These results imply that freestream noise is the mechanism that drives the oscillations for relatively shallow cavities in wind tunnel experiments. This has recently been shown experimentally by use of controlled perturbations in Ref. 16. The implications of this are discussed in more detail later in this section.

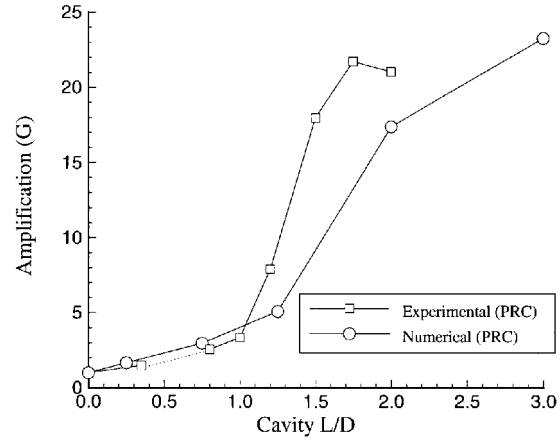

Fig. 5a Amplification vs cavity depth (Mach 5 tunnel).

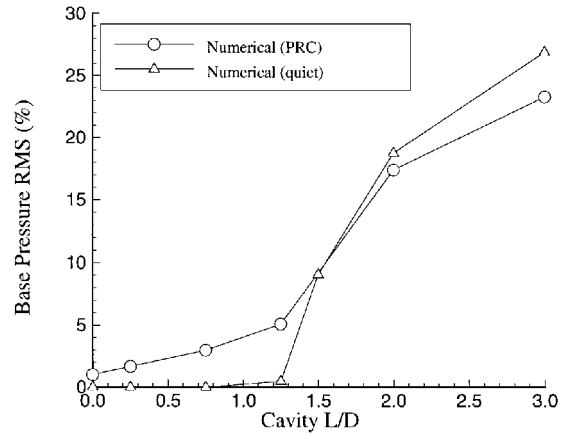

Fig. 5b Base pressure rms vs cavity depth (Mach 5 tunnel).

The numerical results in Fig. 5b, however, also indicate that relatively deep cavities are unstable. Specifically, the deeper cavities resonate strongly without freestream noise. This behavior is termed self-excited resonance. For deep cavities the oscillations are of nearly the same strength regardless of whether inflow noise is included in the simulation.

To further validate the claim that freestream noise is the mechanism that drives resonance in relatively shallow cavities, numerical simulation results are compared with quiet freestream experimental

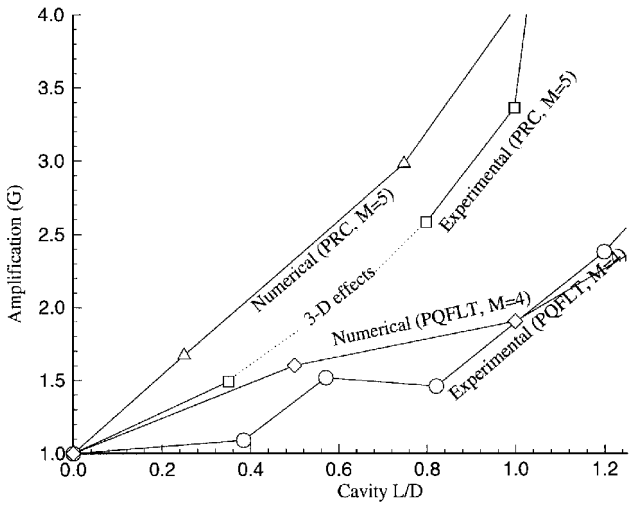

Fig. 6 Amplification vs tunnel noise level and cavity depth (noise levels: PRC, 1.15%; PQFLT, 0.048%).

results obtained in the Mach 4 PQFLT. The experimental inflow noise contains an rms variation of only about ±0.048%, based on rms pitot pressure measurements. The numerical input noise is again adapted from Mach 5 blowdown tunnel measurements except that it is rescaled down by a factor of 24 (from ±1.15%) to obtain the desired rms variation of ±0.048%. Again, more than 50 oscillation cycles are computed for each configuration.

Figure 6 illustrates how the amplification grows with cavity L/D in the numerical simulations and experiments at both Mach 4 (PQFLT) and Mach 5 (PRC). The numerical and experimental results in PQFLT again show a gradual increase of oscillation strength with cavity depth for relatively shallow cavities ($L/D \leq 1.0$). There is no evidence of the two-mode (three-dimensional) behavior mentioned earlier for the Mach 5 experiments in any of the Mach 4 PQFLT results. Note also that the Mach 5 amplification results display a larger rate of increase with cavity depth than the Mach 4 results. Based on sensitivity results of amplification vs Mach number (discussed later), it is expected that amplification is somewhat greater at Mach 5. However, the most important conclusion is that these shallow cavities amplify the inflow noise level by roughly the same amount (within a factor of 2) despite the dramatic difference in tunnel noise levels (factor of 24). Consequently, the strength of oscillations for shallow cavities increases with freestream noise level. These results further suggest that broadband freestream tunnel noise is the mechanism of resonance in shallow cavities.

But what is the sensitivity of rms oscillations to frequency content of noise? Time-accurate simulations of Mach 5 flow over a sharp-lip, $L/D = 0.75$ nose cavity ($f_1 = 3600$ Hz) were conducted using the nominal broadband freestream noise model and a notch filtered freestream noise model (notched from 2400 to 4000 Hz). This filter range was chosen based on a sensitivity study of amplification vs input noise frequency (discussed later) to encompass most of the frequency range to which the cavity is sensitive. Both noise models contain the same 1.15% rms variation. This cavity produces an amplification of roughly 3.0 (200% increase) when driven by broadband freestream noise. However, the cavity has an amplification of 1.3 (30% increase) when driven by the notched filtered freestream noise. These results demonstrate that relatively shallow cavities only resonate strongly if the freestream noise contains energy near the primary mode frequency.

Sensitivity Study Overview

A sensitivity study of relatively shallow cavities ($L/D < 1.25$) is conducted to understand how different parameters affect the strength of oscillations within the cavity. In all sensitivity cases examined, numerical resonance is simulated by input of sinusoidal freestream noise at a discrete frequency.

The nominal case is a medium depth cavity ($L/D = 0.75$) with a sharp lip. The inflow noise peak-to-peak amplitudes of pressure and density are $\pm 0.02 P_\infty$ and $\pm 0.02 \rho_\infty$, respectively. The mean freestream conditions correspond to those in the Mach 5 facility.

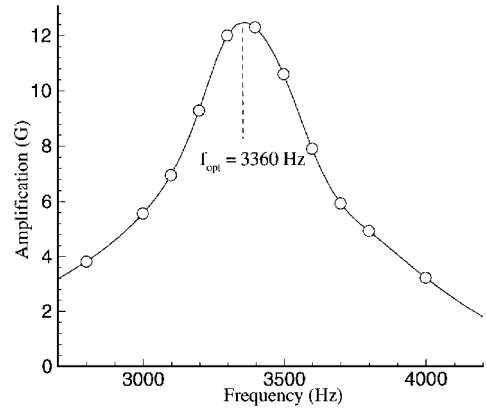

Fig. 7 Amplification vs driving frequency (nominal case).

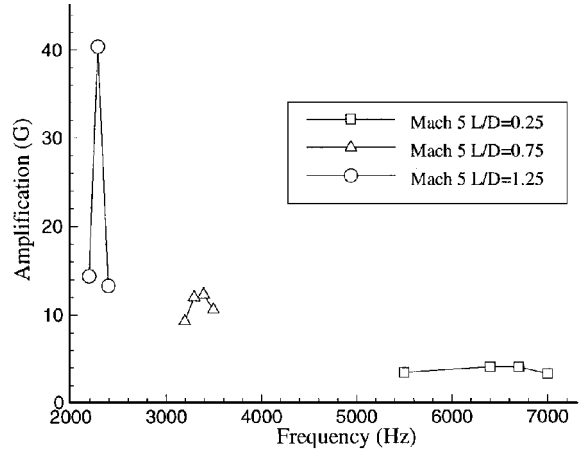

Fig. 8 Peak amplification vs driving frequency.

Note that the freestream rms amplitudes are 1.41%. The simulation results for the nominal case serve as a standard for comparison to the other cases. The parameters studied include noise frequency, noise amplitude, noise variable type, cavity depth, cavity lip radius, Mach number, fluid viscosity, and thermal wall condition.

Sensitivity of Amplification to Noise Frequency

Consider first the dependence of the pressure amplification (G), defined in Eq. (3), on the input perturbation frequency. Figure 7 illustrates the variation of amplification with input frequency f for the nominal case ($L/D = 0.75$ at Mach 5). There is a strong dependence of the amplification on the input frequency. The amplification is maximum when the driving frequency has a particular value (f_{opt}). This optimum frequency is slightly less (8%) than the primary frequency from Eq. (2). The amplification also drops rapidly (rolls off) with changes in the driving frequency, similarly to the behavior of a damped harmonic oscillator.

Figure 8 shows the dependence of amplification on input frequency for three cavity depths ($L/D = 0.25$, 0.75, and 1.25) near the amplification peaks. These peaks become higher and sharper as the cavity depth (and amplification) is increased. The increase of normalized amplification rolloff $|\mathrm{d}G/\mathrm{d}(f/f_{\text{opt}})|$ with amplification is also consistent with a damped harmonic oscillator.

Sensitivity of Amplification to Noise Amplitude

Consider the dependence of amplification on noise level, i.e., input perturbation amplitude. Several simulations are performed for the nominal $L/D = 0.75$ case at each noise amplitude level using different frequencies to isolate f_{opt}. In each case, the same frequency (3400 ± 100 Hz) is identified as this optimum frequency, i.e., f_{opt} is independent of the noise amplitude.

Figure 9 shows the variation of amplification and mean bow-shock speed (averaged over one oscillation cycle) with noise rms level at the optimum frequency. The pressure levels within a given cavity increase nearly proportionally with inflow noise rms until the strength of pressure oscillations begins to plateau or saturate,

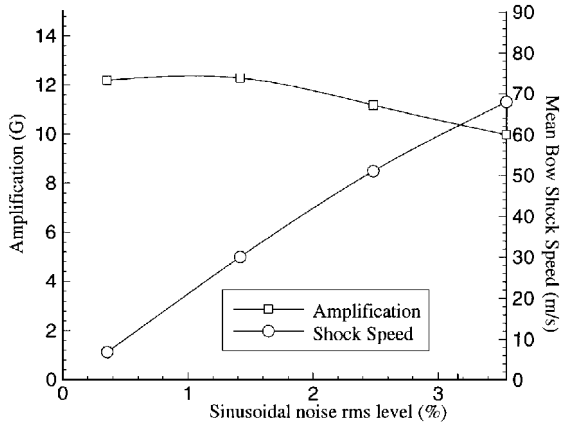

Fig. 9 Amplification and bow-shock speed vs sinusoidal noise level.

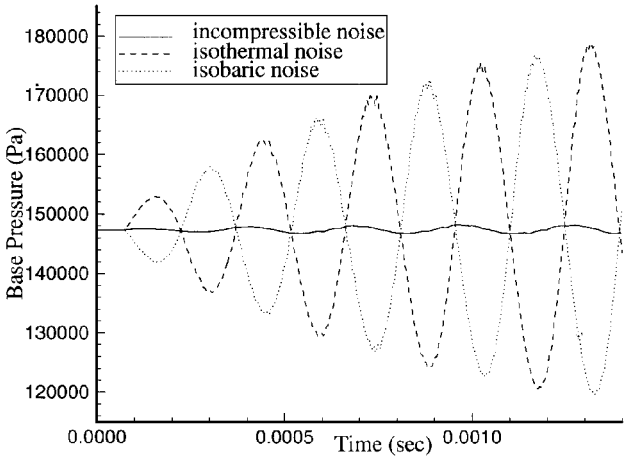

Fig. 10 Base pressure histories for three noise-variable modes (from startup).

i.e., amplification stays nearly constant until saturation occurs at a noise rms level of approximately 1–2%. These results confirm those described earlier in which amplification is shown to be roughly independent of broadband noise amplitude.

The same trend is evident for the variation of mean bow-shock speed with noise amplitude, i.e., mean bow-shock speed increases proportionally to inflow noise rms. Based on the two illustrated relationships, one may deduce that basewall pressure amplitude also increases proportionally to mean bow-shock speed (and bow-shock oscillation amplitude). This relationship implies a stiffness because as the bow-shock oscillation amplitude grows, so does the basewall pressure amplitude.

Sensitivity of Amplification to Noise Variable

Next consider the sensitivity of amplification to the specific choice of noise variable, that is, whether the noise is isothermal, isobaric, or incompressible. As described earlier, the nominal case includes sinusoidal perturbations in pressure and density (isothermal noise). Figure 10 shows the base pressure history (starting from steady flow) for the nominal case at the primary mode frequency (3600 Hz). Base pressure histories are also plotted using two other noise models: isobaric (perturbations in temperature and density) and incompressible (perturbations in pressure and temperature). Both the isothermal and isobaric noise models produce the same amplification (but 180 deg out of phase). Incompressible noise, however, results in negligible oscillations. These trends may be confirmed analytically for small perturbations using normal-shock relations.[18]

Sensitivity of Amplification to Cavity Geometry

Consider the sensitivity of pressure amplification to cavity geometry. Specifically, the sensitivities to cavity depth and cavity lip radius have been studied numerically. Typically, four separate simulations are performed for each geometry using different frequencies to obtain f_{opt}.

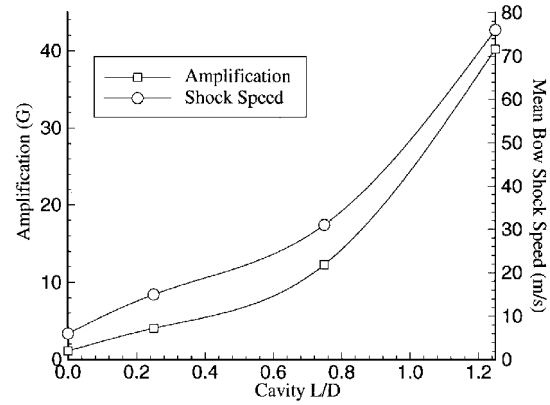

Fig. 11 Amplification and bow-shock speed vs cavity depth.

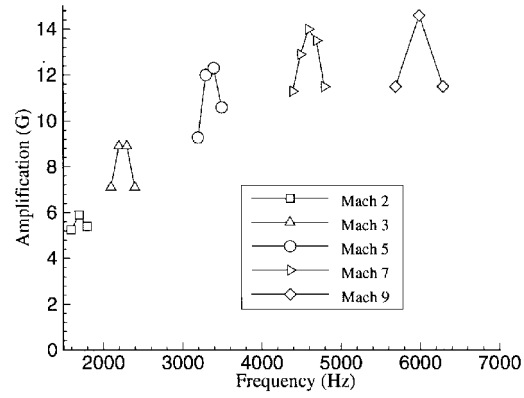

Fig. 12 Peak amplification vs Mach number.

Figure 11 illustrates optimum amplification and mean bow-shock speed relative to the body for four sharp lip cavities with different cavity lengths (other geometry features held constant). A sinusoidal noise amplitude of $\pm 0.5\%$, rather than $\pm 2\%$, is used in these simulations to prevent saturation of pressure oscillation levels. Both amplification and mean bow-shock speed increase monotonically and almost exponentially with cavity length over the entire L/D range.

The effect of geometric scale is studied by comparing the pressure-time history for the nominal $L/D = 0.75$ case at a driving frequency of 3300 Hz with a half-scale version at a driving frequency of 6600 Hz. The resulting pressure–time histories (normalized by frequency) and amplifications (both not shown) are virtually identical, indicating dynamic similarity (no sensitivity to scale). Dynamic similarity is expected because boundary layers and viscous dissipation forces appear to be quite small in these two cases. Of course, boundary-layer effects may be significant at smaller scales.

Pressure oscillations are modestly sensitive to lip geometry for the range of lip radii from 0.1 to 1.0 mm. Experimental results obtained at Mach 5 concluded that flow dynamics near the cavity base are not substantially affected by changes in the lip shape.[9] Numerical simulations using a sinusoidal perturbation at Mach 5 indicate weak to modest sensitivity of the amplification parameter to small changes in lip radius. The amplification for $L/D = 0.25$ and 0.75 increases approximately 5 and 25%, respectively, as the lip radius is varied between 0.1 and 1.0 mm.

Sensitivity of Amplification to Mach Number

Consider next the effect of Mach number on pressure amplification. Numerical simulations are performed using the geometrically nominal $L/D = 0.75$ case but at different Mach numbers. In each simulation, adiabatic wall conditions are implemented and the flow is assumed calorically perfect. Three or four separate simulations are performed for each Mach number using different frequencies to isolate f_{opt}.

Figure 12 shows the variation of amplification with input frequency for Mach 2, 3, 5, 7, and 9. The results indicate that

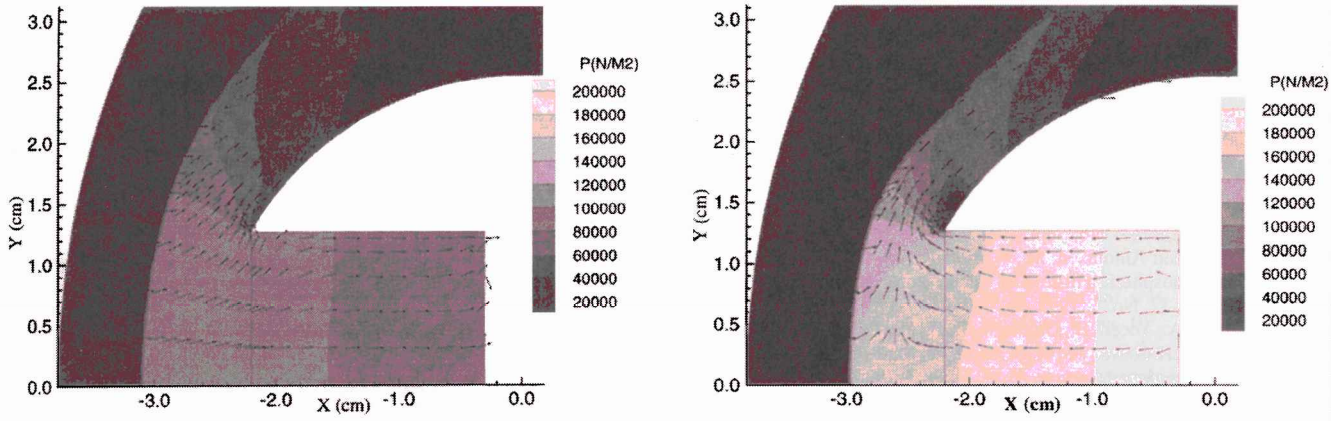

a) Cavity inflow, shock moving aft

b) Cavity outflow, shock moving forward

Fig. 13 Pressure contours (arrows indicate flow direction): L/D = 0.75, Mach 5, 5% sinusoid.

amplification increases rapidly with Mach number for low Mach numbers but begins to level off at hypersonic speeds.

Sensitivity of Amplification to Viscous Effects

The effect of fluid viscosity was studied by comparing the base pressure history for the nominal $L/D = 0.75$ case with the same case, but including an inviscid fluid constraint, i.e., viscosity = 0. The inviscid solution was virtually identical (not shown) to the nominal viscous solution indicating that the primary dissipation mechanism is not a viscous phenomenon in these cases.

Sensitivity of Amplification to Thermal Constraint

Simulation results indicate that the thermal wall constraint, i.e., isothermal wall vs adiabatic wall, has a weak effect on amplification for cases that involve a small temperature potential, i.e., the wall temperature is close to the stagnation temperature. For example, the nominal $L/D = 0.75$ case ($T_0 = 370$ K) with an isothermal wall at 300 K shows a reduction in the amplification of less than 2% if an adiabatic wall is used instead.

However, if the temperature potential is large, amplification is significantly reduced. Simulation results for the nominal geometric configuration at Mach 9 with isothermal wall (300 K) and adiabatic wall conditions showed a 30% reduction in amplification in the isothermal wall case. Perhaps the large radial temperature gradients within the cavity cause the resonant frequency to become a strong function of radial position, and this ambiguity leads to significantly reduced amplification.

Overview of Cavity Fluid Dynamics

As described earlier, inflow noise drives oscillations within shallow cavities; without noise the cavities do not oscillate. Time-accurate flow animations show the fluid-dynamic mechanism by which resonance is achieved. Consider a nose-cavity flow simulation involving a sinusoidal model of inflow noise. During one half cycle, the freestream stagnation pressure is larger than the mean value. This positive freestream perturbation results in a larger inflow momentum (and stagnation pressure) reaching the cavity mouth. This relatively large momentum encourages cavity inflow (and increases the pressure gradient within the cavity). During cavity inflow, the bow shock is moving downstream, toward the cavity mouth (Fig. 13a). Similarly, negative freestream perturbations result in a smaller inflow momentum (and stagnation pressure) reaching the mouth. This relatively small momentum encourages cavity outflow (and decreases the pressure gradient within the cavity). During cavity outflow, the bow shock is moving upstream, away from the cavity mouth (Fig. 13b). Cavity flow reversals occur after each half cycle. These observations indicate how freestream flow momentum (or stagnation pressure) perturbations could be the driving force behind the oscillations.

During startup, i.e., the first several cycles, both the strength of the pressure oscillations inside the cavity and the bow-shock oscillations grow with each input cycle. The basewall pressure oscillations and bow-shock oscillations are nearly in phase. Eventually, a pseudo-steady-state variation of pressure is reached.

The response of the cavity to inflow noise is analogous to that of a damped harmonic oscillator (see also Ref. 16). An attempt to emulate cavity behavior with a spring–mass–damper model based on physical principles has been presented in Ref. 18. An enhanced version of this spring–mass–damper model will be presented in a future publication.

Summary

The agreement shown between computations and experiments implies that freestream noise in a small bandwidth of frequencies near the primary mode is the mechanism that drives resonant pressure oscillations within shallow forward-facing cavities. On the other hand, numerical simulations indicate that deep cavities are unstable and will oscillate without freestream noise, i.e., undergo self-excited resonant oscillations. Most of the energy of the oscillations is contained in the primary mode, which can be estimated a priori.

A parametric study of shallow cavities established the sensitivity of amplification (gain) to noise frequency, noise amplitude, noise variable type, cavity depth, cavity lip radius, geometric scale, Mach number, and viscous and thermal wall conditions. The response of shallow cavities to inflow noise is analogous to that of a damped harmonic oscillator.

Acknowledgments

Funding was provided by the Institute for Advanced Technology under Army Research Laboratory Contract DAAA21-93-C0101, monitored by William G. Reinecke. Work in the PQFLT was made possible by the U.S. Air Force Office of Scientific Research under Grant F49620-94-1-0067, by a gift from The Boeing Company, and by a gift in memory of K. H. Hobbie. The authors are grateful to Cray Research, Inc., for use of the Cray Y-MP at the University of Texas, to NASA for use of the Numerical Aerospace Simulation supercomputer center at NASA Ames Research Center, to Scott Imlay of Amtec Engineering for providing technical assistance with the numerical simulations, and to Bulent Yuceil for providing experimental data.

References

[1]Engblom, W. A., and Goldstein, D. B., "Nose-Tip Surface Heat Reduction Mechanism," *Journal of Thermophysics and Heat Transfer,* Vol. 10, No. 4, 1996, pp. 598–606.

[2]Burbank, P. B., and Stallings, R. L., "Heat-Transfer and Pressure Measurements on a Flat-Face Cylinder at a Mach Number Range of 2.49 to 4.44," NASA TMX-221, 1959.

[3]Cooper, M., Beckwith, I. E., Jones, J. J., and Gallagher, J. J., "Heat-Transfer Measurements on a Concave Hemispherical Nose Shape with Unsteady-Flow Effects at Mach Numbers of 1.98 and 4.95," NACA RM L58D25a, July 1958.

[4]Marquart, E. J., Grubb, J. B., and Utreja, L. R., "Bow-Shock Dynamics of a Forward-Facing Nose Cavity," AIAA Paper 87-2709, Oct. 1987.

[5]Huebner, L. D., and Utreja, L. R., "Mach 10 Bow-Shock Behavior of a Forward-Facing Nose Cavity," *Journal of Spacecraft and Rockets,* Vol. 30, No. 3, 1993, pp. 291–297.

[6]Bohachevsky, I. O., and Kostoff, R. N., "Supersonic Flow over a Convex and Concave Shapes with Radiation and Ablation Effects," *AIAA Journal,* Vol. 10, No. 8, 1972, pp. 1024–1031.

[7]Bastianon, R. A., "Unsteady Solution of the Flowfield over Concave Bodies," AIAA Paper 68-946, Sept. 1968.

[8]Yang, H. Q., and Antonison, M., "Unsteady Flowfield over a Forward-Looking Endoatmospheric Hit-to-Kill Interceptor," *Journal of Spacecraft and Rockets,* Vol. 32, No. 3, 1995, pp. 440–444.

[9]Engblom, W. A., Yuceil, B., Goldstein, D. B., and Dolling, D. S., "Experimental and Numerical Study of Hypersonic Forward-Facing Cavity Flow," *Journal of Spacecraft and Rockets,* Vol. 33, No. 3, 1996, pp. 353–359.

[10]Yuceil, B., and Dolling, D. S., "IR Imaging and Shock Visualization of Flow over a Blunt Body with a Nose Cavity," AIAA Paper 96-0232, Jan. 1996.

[11]Imlay, S. T., Roberts, D. W., Soetrisno, M., and Eberhardt, S., "INCA User's Manual," Version 1.1, Amtec Engineering, Bellevue, WA, Jan. 1991.

[12]Steger, J. L., and Warming, R. F., "Flux Vector Splitting of the Gasdynamic Equations with Applications to Finite-Difference Methods," *Journal of Computational Physics,* Vol. 40, No. 2, 1981, pp. 263–293.

[13]Tam, C. K. W., "Computational Aeroacoustics: Issues and Methods," AIAA Paper 95-0677, Jan. 1995.

[14]Schneider, S. P., and Haven, C. E., "Quiet-Flow Ludwieg Tube for High-Speed Transition Research," *AIAA Journal,* Vol. 33, No. 4, 1995, pp. 688–693.

[15]Beckwith, I. E., and Miller, C. G., "Aerothermodynamics in High-Speed Wind Tunnels at NASA Langley," *Annual Review of Fluid Mechanics,* Vol. 22, 1990, pp. 419–439.

[16]Ladoon, D. W., Schmisseur, J. D., and Schneider, S. P., "Laser-Induced Resonance in a Forward-Facing Cavity at Mach 4," AIAA Paper 97-0339, Jan. 1997.

[17]Yuceil, B., "An Experimental Investigation of a Forward-Facing Nose Cavity on a Blunt Body at Mach 5," Ph.D. Dissertation, Dept. of Aerospace Engineering and Engineering Mechanics, Univ. of Texas, Austin, TX, Dec. 1995, pp. 123–132.

[18]Engblom, W. A., "Numerical Investigation of Hypersonic Flow over a Forward-Facing Cavity," Ph.D. Dissertation, Dept. of Aerospace Engineering and Engineering Mechanics, Univ. of Texas, Austin, TX, Aug. 1996, pp. 107–110.

T. C. Lin
Associate Editor